Revision #4

Crystal structure of K-cymrite and kokchetavite from single-crystal X-ray diffraction

Alexandr V. Romanenko[1,2], Sergey V. Rashchenko[1,2], Alexander G. Sokol[1], Andrey V. Korsakov[1], Yurii V. Seryotkin[1,2], Konstantin V. Glazyrin[3], Kira Musiyachenko[1,4]

[1]*Sobolev Institute of Geology and Mineralogy SB RAS, 3 Koptyuga Avenue, 630090 Novosibirsk, Russia*
[2]*Novosibirsk State University, 2 Pirogova Street, 630090 Novosibirsk, Russia*
[3]*Photon Science, Deutsches Elektronen-Synchrotron, Notkestrasse 85, 22607 Hamburg, Germany*
[4]*Department of Earth and Environmental Sciences, University of Pavia, Via A. Ferrata, 1 27100 Pavia, Italy*

Abstract: We determined for the first time the crystal structures of high-pressure K-cymrite ($KAlSi_3O_8 \cdot H_2O$) and its dehydrated form kokchetavite ($KAlSi_3O_8$) using single crystal X-ray diffraction. The structure of K-cymrite has been successfully refined in the hexagonal space group (*P6*/*mmm*, a = 5.3361(3) Å, c = 7.7081(7) Å, V = 190.08(3) Å^3, $R1$ = 0.036 for 127 unique observed reflections) and it is in complete agreement with previous powder X-ray diffraction models. In contrast, kokchetavite shows superstructural reflections, suggesting new values of unit cell and space group *P6*/*mcc* (a = 10.5757(3) Å, c = 15.6404 (6) Å, V = 1514.94(10) Å^3, $R1$ = 0.068 for 1455 unique observed reflections). During dehydration, single-crystal grains of K-cymrite transform into single-crystal grains of kokchetavite. The latter questions a previous interpretation of kokchetavite crystals in mineral inclusions as a product of direct crystallization from fluid/melt. The Raman spectrum of K-cymrite shows a strong polarization dependence, which is important in the identification of the mineral inclusions.

Keywords: K-cymrite, kokchetavite, single-crystal X-ray diffraction, Raman spectroscopy

Introduction

Seki and Kennedy (Seki and Kennedy 1964) showed that, at pressure above 2-3 GPa and temperature between 300-800°C, potassium feldspar reacts with water and forms a high-pressure hydrated phase ($KAlSi_3O_8 + H_2O \rightarrow KAlSi_3O_8 \cdot H_2O$). The structure of the latter was originally thought to be hexagonal, due to the similarity of its X-ray powder diffraction pattern and stoichiometry with those of cymrite (IMA-1949; $BaAl_2Si_2O_8 \cdot H_2O$; Smith et al. 1949; Runnells 1964). The $KAlSi_3O_8 \cdot H_2O$ was also obtained by Huang and Wyllie (Huang and Wyllie 1975) while studying melting reactions in the system $NaAlSi_3O_8$-$KAlSi_3O_8$-SiO_2 at 3.5 GPa and 695°C with an excess of water, and was referred as 'sanidine hydrate'. In further works conducted by Schreyer and Massone (Schreyer 1987; Massone 1992) this phase was referred as 'K-cymrite' – the most used name since then. K-cymrite was also obtained as a product of muscovite decomposition at 800°C between 1.8 and 3.7 GPa with co-formation of $KAlSi_3O_8$-sanidine, Al_2O_3-corundum, and H_2O (Faust and Knittle 1994). Later Fasshauer *et al*. (Fasshauer et al. 1997) carried out a Rietveld refinement of K-cymrite structure using hexagonal $BaAl_2Si_2O_8 \cdot H_2O$ cymrite model with *P6*/*mmm* space group. More recently, Thompson *et al*. (Thompson et al. 1998) obtained a dehydrated form of K-cymrite, originally referred as 'hexasanidine'.

K-cymrite and 'hexasanidine' were identified as mineral inclusions in ultrahigh-pressure rocks from the Kokchetav complex (Mikhno et al. 2013; Hwang et al. 2004); 'hexasanidine' was then approved as *kokchetavite* mineral (IMA-2004-011). In the absence of single-crystal X-ray diffraction data, the *P6/mmm* space group was proposed for kokchetavite (Thompson et al. 1998;

This is the peer-reviewed, final accepted version for American Mineralogist, published by the Mineralogical Society of America.
The published version is subject to change. Cite as Authors (Year) Title. American Mineralogist, in press.
DOI: https://doi.org/10.2138/am-2020-7407. http://www.minsocam.org/

Hwang et al. 2004), again by analogy with the hexagonal model of $BaAl_2Si_2O_8 \cdot H_2O$ cymrite structure. Interestingly, Bolotina *et al*. showed from single-crystal X-ray diffraction data that the structure of $BaAl_2Si_2O_8 \cdot H_2O$ cymrite, used as the model for K-cymrite and kokchetavite structures, is actually monoclinic pseudoorthorhombic (Drits and Kashaev 1968; Bolotina et al. 1991, 2010).

However, current structural models of K-cymrite and kokchetavite are still based on the obsolete hexagonal $BaAl_2Si_2O_8 \cdot H_2O$ cymrite model, being verified only by powder X-ray diffraction and TEM. Here we present the first *ab initio* solution of K-cymrite and kokchetavite crystal structures from single-crystal X-ray diffraction data and solve the ambiguity of their actual symmetry.

Experimental

Synthesis

K-cymrite ($KAlSi_3O_8 \cdot H_2O$)

A charge of $KAlSi_3O_8$ glass-ceramics was obtained by solid state synthesis from K_2CO_3, Al_2O_3, and SiO_2. The reagents were weighted in stoichiometric proportions and then pressed into pellets. The obtained pellets were annealed at 1100°C for one day and then cooled by switching off the furnace.

Experiments at 6.3 GPa and 1000°C (duration of 150 hours) were carried out in a split-sphere multi-anvil high-pressure apparatus (Palyanov et al. 2010). The size of pressure cells was 21.1×21.1×25.4 mm; the graphite heaters in the high pressure runs had an inner diameter of 12 mm and a height of 18.5 mm. Pressure was calibrated by recording the change in the resistance of Bi at 2.55 GPa and PbSe at 4.0 and 6.8 GPa at room temperature and at 1350°C by bracketing the graphite-diamond equilibrium in the $Ni_{0.7}$-$Fe_{0.3}$-C system. Temperature was monitored in each experiment with a $PtRh_6/PtRh_{30}$ thermocouple calibrated at 6.3 GPa using the melting points of Al and Ag (Sokol et al. 2015). Pressure and temperature were measured to an accuracy of ±0.1 GPa and ±20°C, respectively (Palyanov et al. 2010; Sokol et al. 2015). The samples of $KAlSi_3O_8$ glass-ceramics and liquid water in stoichiometric proportion were placed in Pt capsules with a 2 mm outer diameter and a wall thickness of 0.2 mm and then were arc-welded using a Lampert Werktechnik GmbH PUK-4U impulse micro welding. As a result, crystals of K-cymrite approximately 30-70 μm in diameter were obtained (Fig. 1).

Kokchetavite $KAlSi_3O_8$

Kokchetavite was synthesized by the dehydration of K-cymrite using Mettler TA3000 equipment by heating up to 750°C with heating rate 10°C/min. Total weight loss was 6.9 wt%, which slightly exceeds the weight percentage of H_2O equivalent to one H_2O molecule per formula unit (6.07 wt%). The latter may be explained by a low accuracy of the measurement due to small mass of the sample and the presence of absorbed water. The maximum water loss occurs at a temperature close to 500°C (Fig. 2), which is consistent with the data of Thompson *et al*. (Thompson et al. 1998). Interestingly, polarized light microscopy and X-ray diffraction (see below) showed that K-cymrite retain single-crystalline state upon transformation to kokchetavite, suggesting a high permeability of the crystal structure for water molecules.

Chemical analysis

The composition of obtained K-cymrite was investigated using a MIRA 3 LMU scanning electron microscope (Tescan Orsay Holding, 20 kV accelerating voltage and 1.5 nA beam current) coupled with an INCA 450 energy-dispersive X-ray microanalysis system equipped with a liquid nitrogen-free large area EDS X-Max-80 Silicon Drift Detector (Oxford Instruments Nanoanalysis Ltd) at IGM SB RAS.

The average of 33 analyses of 8 grains of the K-cymrite is: SiO_2 61(1.3) wt.%, Al_2O_3 17.1(5) wt.%, K_2O 15.3(3) wt.% (sum 93.59% wt.%). After normalizing to eight oxygens, we obtained the following formula: $K_{0.96(2)}Al_{1.01(1)}Si_{3.01(1)}O_8 \cdot H_2O$. We did not observe any variations of chemical composition between different grains and inhomogeneities across a grain exceeding the measurement error.

Single-crystal X-ray diffraction

K-cymrite ($KAlSi_3O_8 \cdot H_2O$)

A 0.07×0.05×0.03 mm^3 crystal of K-cymrite was selected for X-ray diffraction measurements using polarizing microscope (no evidence of twinning was observed). The measurements were performed on an Oxford Diffraction Gemini Ultra R diffractometer with a CCD detector (MoKα radiation, λ = 0.71073 Å, graphite monochromator, ω scan, scan step 1°, exposure 60 s per frame). The X-ray diffraction data set was processed with the CrysAlis^{Pro} software; the structure was solved by a direct method and refined using the SHELXL program package (Hübschle et al. 2011; Sheldrick 2015); a missing symmetry was checked using the PSEUDO tool of Bilbao Crystallographic Server (Capillas et al. 2011). The details of data collection and refinement, as well as refined positional parameters, are listed in Tables 1 and 2, respectively (see also a supplementary CIF). Crystal structure drawings were prepared using the VESTA software (Momma and Izumi 2011).

Kokchetavite ($KAlSi_3O_8$)

Kokchetavite single crystals obtained by dehydration of K-cymrite were also studied by single-crystal X-ray diffraction. However, the quality of crystals deteriorated after dehydration, which did not allow us to collect satisfactory data using a laboratory diffractometer. The crystal selection and diffraction data collection were therefore performed at P02.2 beamline of Deutsches Elektronen-Synchrotron (DESY). X-ray diffraction measurements were performed at a wavelength of 0.2897 Å (42.7 keV) with a beam size of 8×3 μm (Liermann et al. 2015). Diffraction patterns were collected using the fast area detector XRD 1621 (PerkinElmer) during ±30° rotation of the 0.04×0.03×0.02 mm^3 crystal (ω scan, scan step 0.5°, exposure 1 s per frame). The patterns were then transferred into the CrysAlis^{Pro} software using the ESPERANTO protocol (Rothkirch et al. 2013) for indexing and integration. All subsequent procedures to solve and refine the structure were carried out in the same way as for K-cymrite. Atomic scattering factors and photoabsorption coefficients were given from the NIST Standard Reference Database 66 (Chantler 1995) for an energy of 41.8 keV. Details of the data collection and refinement, as well as the positional parameters are listed in Tables 1 and 2, respectively (see also a supplementary CIF).

Raman spectroscopy

Raman measurements of K-cymrite ($KAlSi_3O_8 \cdot H_2O$) and kokchetavite ($KAlSi_3O_8$) were performed using a Horiba Jobin Yvon LabRAM HR800 Raman spectrometer with a 532-nm solid state laser. Spectra were recorded at ambient conditions in backscattering geometry with a

This is the peer-reviewed, final accepted version for American Mineralogist, published by the Mineralogical Society of America.
The published version is subject to change. Cite as Authors (Year) Title. American Mineralogist, in press.
DOI: https://doi.org/10.2138/am-2020-7407. http://www.minsocam.org/

laser power of about 1 mW and a spectral resolution of approximately 2 cm^{-1} (Fig. 3). The obtained Raman spectra of the samples correspond to K-cymrite and kokchetavite (Kanzaki et al. 2012). No other phases were detected except for coesite as micro-inclusions.

K-cymrite has a distinct cleavage perpendicular to the *c* axis (see Fig. 3), so Raman spectra can be easily measured at different orientations of sample. We measured a polarization dependence of 833 cm^{-1} and OH-region bands intensities (Fig. 3) in the following orientations (Porto's notation):

–Z(XX)Z
–X(ZZ)X
–X(YY)X

According to the Raman selection rules for the point group 6/*mmm*, A_{1g} mode is allowed in all orientations, while E_{2g} modes only in the orientations –Z(XX)Z and –X(YY)X. We do not observe the 833 cm^{-1} band nor any intensities in the OH region in the orientation –X(ZZ)X which indicates that the symmetry of these vibrations is E_{2g}. The presence of the line 381 cm^{-1} in all orientations suggest the A_{1g} symmetry.

Assuming that peak in OH-region is related to the stretching of O-H covalent bond, the observed polarization dependence suggests that the orientation of such bonds should be nearly perpendicular to [001]. The same polarization dependence of 833 cm^{-1} band related to T-O-T bending oscillations suggests its origin as asymmetric T-O2-T bending perpendicular to [001] (Fig. 3a).

The Raman spectrum of kokchetavite in general resembles that of K-cymrite, however, all the main bands are shifted and no stretching OH-modes are observed matching with the data of Kanzaki et al.

Results and discussion

Structure and symmetry of K-cymrite ($KAlSi_3O_8 \cdot H_2O$)

In contrast to $BaAl_2Si_2O_8 \cdot H_2O$ cymrite, K-cymrite can be successfully refined in the hexagonal space group (*P*6/*mmm*, a = 5.3361(3), c = 7.7081(7)) matching the historically used model (see Table 1).

The structure of K-cymrite is based on double layers of Al- and Si- tetrahedra (no NMR evidence of Al/Si ordering was reported by Fasshauer et al. and Kanzaki et al) with interlayer K cations (Fig. 4). The double layer consists of regular six-membered rings. In the (001) plane, each ring is connected to six adjacent ones. Along the [001] direction, the rings are connected by shared apical oxygens (O2 site) forming a double layer; the voids in the double layer are populated by water molecules disordered along the *c* axis (Fig. 4).

We do not observe any evidence of deviation of K-cymrite symmetry from hexagonal, such as twinning and satellite reflexions typical for monoclinic pseudoorthorhombic-pseudohexagonal $BaAl_2Si_2O_8 \cdot H_2O$ cymrite. However, a certain ambiguity exists regarding presence of inversion center in K-cymrite structure, *i.e.* choice between *P*6/*mmm* space group and its non-centrosymmetric *P622* and *P–62m* subgroups. Structure refinement in the non-centrosymmetric subgroups did not result in a noticeable improvement of the wR^2-factor, and also suffered from

large correlation between positional parameters, so that *P*6/*mmm* was chosen as the most reliable space group for K-cymrite.

The six shared apical oxygens in O2 sites surround Ow water molecule at a distance Ow-O2 = 3.0951(13) Å sufficient to form hydrogen bonds (Fig 5a, b). As a result, covalent OH-bonds of water molecule become oriented in (001) plane, which agrees well with the data of polarized Raman spectroscopy and the frequency of OH-band at 3545 cm^{-1}, corresponding to Ow-O distance about 3.1 Å (Libowitzky 1999). The hydrogen bonds restrict the Ow-O2 distances and thus restrict the ring deformation and a decrease in symmetry.

180° T-O-T angles in K-cymrite ($KAlSi_3O_8 \cdot H_2O$)

A T-O-T angle of 180°, observed for shared apical oxygens (O2 site) in K-cymrite structure, is often considered as unfavourable for silicates. On the other hand, in a number of structures shared apical oxygen atoms occupy special positions, making the T-O-T angle exactly 180° (Liebau 1985). The relaxation of this angle is possible either via decrease in symmetry (or local symmetry), or via T-O-T bending oscillation around average position. In order to relax the special position restriction, we refined the K-cymrite structure in the orthorhombic subgroup *Cmmm* of the group *P*6/*mmm*. The refined T-O2-T value of 179.8(3), however, is identical to 180° within uncertainty. On the other hand, the static 180° angle of T-O2-T obtained from X-ray diffraction may actually represent a time average of T-O2-T bending. The latter assumption is strongly supported by polarization dependence of Raman band at 833 cm^{-1}, allowing its interpretation as asymmetric T-O2-T bending perpendicular to [001], caused by the deviation of the T-O2-T angle from 180°.

Structure and symmetry of kokchetavite ($KAlSi_3O_8$)

In previous studies, the same *P*6/*mmm* space group and unit cell dimensions close to that of K-cymrite, were proposed for kokchetavite (Thompson et al. 1998; Hwang et al. 2004), again by analogy with the structure of $BaAl_2Si_2O_8 \cdot H_2O$ cymrite. However, our single-crystal X-ray diffraction data shows superstructural reflections in the reciprocal space (Fig. 6), indicating a space group *P*6/*mcc* with doubled *a* and *c* parameters.

Interestingly, the symmetry decrease during K-cymrite → kokchetavite transformation corresponds to the following group-subgroup sequence

$$P6/mmm - i4,\ a'=2a,\ c'=c \rightarrow P6/mmm - k2,\ c'=2c \rightarrow P6/mcc$$

with intermediate fourfold *P*6/*mmm* cell. Since K-cymrite → kokchetavite transition cannot be regarded as second order one due to the loss of H_2O molecules, the existence of corresponding intermediate phase is not necessary (but not excluded). On the other hand, if kokchetavite-like structure with distorted tetrahedral rings could be stabilized in hydrated form (*e.g.* at high pressure), the intermediate phase would probably appear in the course of corresponding transition.

The difference of *V*/*Z* value between kokchetavite and K-cymrite is 0.71 $Å^3$ (-0.3%). Similarly to previous works (Thompson et al. 1998; Hwang et al. 2004), we observe an expansion along the *c* direction (+1.5%) and a contraction along *a* direction (-0.9%) compared to K-cymrite.

In contrast to the structure of K-cymrite where hydrogen bonds restrict the Ow-O2 distances and so prevent deformation of regular tetrahedral rings, two types of rings exist in kokchetavite

structure: distorted and regular, withlatter surrounded by six distorted ones (Fig. 4). Interatomic distances and bond angles for kokchetavite structure are given in the Table 3.

Implications

Identification of K-cymrite and kokchetavite in natural samples

K-cymrite and kokchetavite, along with coesite and diamond, are indicators of ultrahigh-pressure metamorphism (UHPM) of crustal rocks. Due to the large anisotropy of K-cymrite and kokchetavite structure, vibrational spectra strongly depend on the orientation of the sample (Fig. 3), which should be taken into account during identification of these phases in mineral inclusions. For example, this explains an 'enigmatic' absence of 833 cm^{-1} band of K-cymrite reported by Mikhno *et al*. (Mikhno et al. 2013) in some spectra.

Single-crystal grains inside fluid/melt inclusions are usually interpreted as direct crystallization products from fluid/melt. However, during dehydration, single-crystal grains of K-cymrite transforms to single-crystal grains of kokchetavite, which limits the applicability of such interpretation.

The role of K-cymrite and kokchetavite as potassium and fluid carrier into the mantle

Subduction zones are considered giant conveyor belts that strongly affects chemistry of the deep Earth. However, the oceanic crust itself is depleted in natural radioactive isotopes (K, U and Th) (Maruyama et al. 2013), and so cannot be regarded the main carrier of such elements into the mantle. However, field observations of K-rich rocks in ultrahigh-pressure metamorphic terranes exhumed from the depths of ~200 km (Mikhno et al. 2013) suggest that K transport into the mantle effectively occurs, and its possible mechanisms are (a) subduction of microcontinents and (b) 'scratching' of K-rich continental crust by subducting plates. Subducted K-rich rocks may accumulate near the mantle transition zone, where they act as a source of radiogenic heat due to their high concentration of K, U and Th (Safonova et al. 2015). Since potassium feldspar is a ubiquitous mineral in the Earth's crust, K-cymrite and kokchetavite should widely form during ultrahigh-pressure metamorphism (UHPM) with the participation of fluids (Seki and Kennedy 1964; Fasshauer et al. 1997; Thompson et al. 1998). This assumption is confirmed by the findings of K-cymrite and kokchetavite as inclusions in minerals from different crustal high-pressure complexes (Hwang et al. 2004, 2009; Zhang et al. 2009; Mikhno et al. 2013; Ferrero et al. 2016).

The existence of K-cymrite and kokchetavite should be taken into account in thermodynamical models of subducting processes. However, this requires a knowledge of the thermodynamic properties of K-cymrite and kokchetavite which may be calculated by *ab intio* methods using crystal structures reported in this article.

Materials for fluids storage and probe for deep fluid chemistry

Findings of hydrated (K-cymrite) and dehydrated (kokchetavite) forms of high-pressure $KAlSi_3O_8 \cdot H_2O$ suggest that the occurrence of these phases strongly depend on the activity of the fluid. Sokol *et al*. (Sokol et al. 2019) showed that host-guest interaction between Al-Si 'framework' and fluid components makes possible the formation of H_2O-, N_2-, NH_3-, and NH_4^+-substituted forms. This fact allows the use of K-cymrite as a probe for deep fluids chemistry similarly to cordierite (Harley et al. 2002).

Since K-cymrite is able to keep its crystalline state after dehydration as well as host different species of fluids in the crystal structure (Sokol et al. 2019), materials with similar structure (Hawthorne et al. 2019) can be prospective sorbents and/or catalysts: $BaAl_2Si_2O_8$, hexacelsian (Galuskina et al. 2017), $Pb_2(Fe^{3+}Te^{6+})[AlSi_3O_8]O_6$, burckhardtite (Christy et al. 2014), $CaAl_2Si_2O_8$, dmisteinbergite (Zolotarev et al. 2019), $Ba_{12}(Si_{11}Al_5)O_{31}(CO_3)_8Cl_5$, kampfite (Basciano and Groat 2007).

Acknowledgements:

We acknowledge DESY (Hamburg, Germany), a member of the Helmholtz Association HGF, for the provision of experimental facilities. Parts of this research were carried out at PETRA III, P02.2 Extreme conditions beamline, proposal #I-20181033. We would like to thank Konstantin A. Kokh for providing sanidine glass-ceramics and Mattia Gilio for productive discussion. This study is supported by the Russian Scientific Foundation (project 18-17-00186). A major part of the analytical procedures was carried out at the Analytical Center for multielemental and isotope research, Sobolev Institute of Geology and Mineralogy, Siberian Branch of the Russian Academy of Sciences (IGM SB RAS), Novosibirsk, Russia. A.G. Sokol work on K-cymrite synthesis was supported by state assignment of IGM SB RAS.

References:

Basciano, L.C., and Groat, L.A. (2007) The crystal structure of kampfite. The Canadian Mineralogist, 45, 935–943.

Bolotina, N.B., Rastsvetaeva, R.K., Andrianov, V.I., and Kashaev, A.A. (1991) Refinement of modulated crystals: structure of cymrite. Soviet physics. Crystallography, 36, 190–194.

Bolotina, N.B., Rastsvetaeva, R.K., and Kashaev, A.A. (2010) Refinement of the twinned structure of cymrite from the Ruby Creek deposit (Alaska). Crystallography Reports, 55, 569–574.

Capillas, C., Tasci, E.S., F.G., Orobengoa, D., Perez-Mato, J.M., and Aroyo, M.I. (2011) A new computer tool at the Bilbao Crystallographic Server to detect and characterize pseudosymmetry. Zeitschrift für Kristallographie Crystalline Materials, 226, 186–196.

Chantler, C.T. (1995) Theoretical Form Factor, Attenuation, and Scattering Tabulation for Z =1–92 from E =1–10 eV to E =0.4–1.0 MeV. Journal of Physical and Chemical Reference Data, 24, 71–643.

Christy, A.G., Kampf, A.R., Mills, S.J., Housley, R.M., and Thorne, B. (2014) Crystal structure and revised chemical formula for burckhardtite, $Pb_2(Fe^{3+}Te^{6+})[AlSi_3O_8]O_6$: a double-sheet silicate with intercalated phyllotellurate layers. Mineralogical Magazine, 78, 1763–1773.

Drits, V.A. and Kashaev, A.A. (1968) The origin of satellites in the reciprocal lattice of cymrite. Soviet Physics - Crystallography, 13, 700–705.

Fasshauer, D.W., Chatterjee, N.D., and Marler, B. (1997) Synthesis, structure, thermodynamic properties, and stability relations of K-cymrite, K [AlSi 3 O 8]· H 2 O. Physics and Chemistry of Minerals, 24, 455–462.

Faust, J., and Knittle, E. (1994) The equation of state, amorphization, and high-pressure phase diagram of muscovite. Journal of Geophysical Research: Solid Earth, 99, 19785–19792.

Ferrero, S., Ziemann, M.A., Angel, R.J., O'Brien, P.J., and Wunder, B. (2016) Kumdykolite, kokchetavite, and cristobalite crystallized in nanogranites from felsic granulites, Orlica-Snieznik Dome (Bohemian Massif): not evidence for ultrahigh-pressure conditions. Contributions to Mineralogy and Petrology, 171.

Galuskina, I.O., Galuskin, E.V., Vapnik, Y., Prusik, K., Stasiak, M., Dzierżanowski, P., and Murashko, M. (2017) Gurimite, $Ba_3(VO_4)_2$ and hexacelsian, $BaAl_2Si_2O_8$ – two new minerals from schorlomite-rich paralava of the Hatrurim Complex, Negev Desert, Israel. Mineralogical Magazine, 81, 1009–1019.

Harley, S.L., Thompson, P., Hensen, B.J., and Buick, I.S. (2002) Cordierite as a sensor of fluid conditions in high-grade metamorphism and crustal anatexis: cordierite, metamorphism and anatexis. Journal of Metamorphic Geology, 20, 71–86.

Hawthorne, F.C., Uvarova, Y.A., and Sokolova, E. (2019) A structure hierarchy for silicate minerals: sheet silicates. Mineralogical Magazine, 83, 3–55.

Huang, W.-L., and Wyllie, P.J. (1975) Melting Reactions in the System $NaAlSi_3O_8$-$KAlSi_3O_8$-SiO_2 to 35 Kilobars, Dry and with Excess Water. The Journal of Geology, 83, 737–748.

Hübschle, C.B., Sheldrick, G.M., and Dittrich, B. (2011) *ShelXle* : a Qt graphical user interface for *SHELXL*. Journal of Applied Crystallography, 44, 1281–1284.

Hwang, S.L., Shen, P.Y., Chu, H.T., Yui, T.F., Liou, J., Sobolev, N.V., Zhang, R.Y., Shatsky, V.S., and Zayachkovsky, A.A. (2004) Kokchetavite: a new potassium-feldspar polymorph from the Kokchetav ultrahigh-pressure terrane. Contributions to Mineralogy and Petrology, 148, 380–389.

Hwang, S.-L., Shen, P., Chu, H.-T., Yui, T.-F., Liou, J.G., and Sobolev, N.V. (2009) Kumdykolite, an orthorhombic polymorph of albite, from the Kokchetav ultrahigh-pressure massif, Kazakhstan. European Journal of Mineralogy, 21, 1325–1334.

Libowitzky, E. (1999) Correlation of OH stretching frequencies and OH O hydrogen bond lengths in minerals. In Hydrogen Bond Research pp. 103–115. Springer.

Liebau, F. (1985) Structural Chemistry of Silicates: Structure, Bonding, and Classification. Springer-Verlag, Berlin Heidelberg.

Liermann, H.-P., Konôpková, Z., Morgenroth, W., Glazyrin, K., Bednarčik, J., McBride, E.E., Petitgirard, S., Delitz, J.T., Wendt, M., Bican, Y., and others (2015) The Extreme Conditions Beamline P02.2 and the Extreme Conditions Science Infrastructure at PETRA III. Journal of Synchrotron Radiation, 22, 908–924.

Maruyama, S., Ikoma, M., Genda, H., Hirose, K., Yokoyama, T., and Santosh, M. (2013) The naked planet Earth: Most essential pre-requisite for the origin and evolution of life. Geoscience Frontiers, 4, 141–165.

Massonne, H.-J. (1992) Evidence for low-temperature ultrapotassic siliceous fluids in subduction zone environments from experiments in the system K_2O-MgO-Al2O_3-SiO_2-H_2O (KMASH). Lithos, 28, 421–434.

McKeown, D.A., Bell, M.I., and Etz, E.S. (1999) Raman spectra and vibrational analysis of the trioctahedral mica phlogopite. American Mineralogist, 84, 970–976.

Mikhno, A.O., Schmidt, U., and Korsakov, A.V. (2013) Origin of K-cymrite and kokchetavite in the polyphase mineral inclusions from Kokchetav UHP calc-silicate rocks: evidence from confocal Raman imaging. European Journal of Mineralogy, 25, 807–816.

Momma, K., and Izumi, F. (2011) VESTA 3 for three-dimensional visualization of crystal, volumetric and morphology data. Journal of Applied Crystallography, 44, 1272–1276.

Palyanov, Y.N., Borzdov, Y.M., Khokhryakov, A.F., Kupriyanov, I.N., and Sokol, A.G. (2010) Effect of Nitrogen Impurity on Diamond Crystal Growth Processes. Crystal Growth & Design, 10, 3169–3175.

Rothkirch, A., Gatta, G.D., Meyer, M., Merkel, S., Merlini, M., and Liermann, H.-P. (2013) Single-crystal diffraction at the Extreme Conditions beamline P02.2: procedure for collecting and analyzing high-pressure single-crystal data. Journal of Synchrotron Radiation, 20, 711–720.

Runnells, D.D. (1964) Cymrite in a copper deposit, brooks range, Alaska. American Mineralogist, 49, 158–165.

Safonova, I., Litasov, K., and Maruyama, S. (2015) Triggers and sources of volatile-bearing plumes in the mantle transition zone. Geoscience Frontiers, 6, 679–685.

Schreyer, W. (1987) Continental crust subducted to depths near 100 km: Implications for magma and fluid genesis in collision zones. Magmatic Processes: Physicochemical Principles, 1, 10.

Seki, Y., and Kennedy, G.C. (1964) The breakdown of potassium feldspar, $KAlSi_3O_8$ at high temperatures and high pressures. American Mineralogist, 49, 1688–1706.

Sheldrick, G.M. (2015) Crystal structure refinement with SHELXL. Acta Crystallographica, Section C: Structural Chemistry, 71, 3–8.

Smith, W.C., Bannister, F.A., and Hey, M.H. (1949) Cymrite, a new barium mineral from the Benallt manganese mine, Rhiw, Carnarvonshire. Mineralogical Magazine and Journal of the Mineralogical Society, 28, 676–681.

Sokol, A.G., Borzdov, Y.M., Palyanov, Y.N., and Khokhryakov, A.F. (2015) High-temperature calibration of a multi-anvil high pressure apparatus. High Pressure Research, 1–9.

Sokol, A.G., Kupriyanov, I.N., Seryotkin, Y.V., Sokol, E.V., Kruk, A.N., Tomilenko, A.A., Bul'bak, T.A., and Palyanov, Y.N. (2019) Cymrite as Mineral Clathrate: An Overlooked Redox Insensitive Transporter of Nitrogen in the Mantle. Gondwana Research.

Thompson, P., Parsons, I., Graham, C.M., and Jackson, B. (1998) The breakdown of potassium feldspar at high water pressures. Contributions to Mineralogy and Petrology, 130, 176–186.

Zhang, R.Y., Liou, J.G., Iizuka, Y., and Yang, J.S. (2009) First record of K-cymrite in North Qaidam UHP eclogite, Western China. American Mineralogist, 94, 222–228.

Zolotarev, A.A., Krivovichev, S.V., Panikorovskii, T.L., Gurzhiy, V.V., Bocharov, V.N., and Rassomakhin, M.A. (2019) Dmisteinbergite, $CaAl_2Si_2O_8$, a Metastable Polymorph of Anorthite: Crystal-Structure and Raman Spectroscopic Study of the Holotype Specimen. Minerals, 9, 570.

This is the peer-reviewed, final accepted version for American Mineralogist, published by the Mineralogical Society of America.
The published version is subject to change. Cite as Authors (Year) Title. American Mineralogist, in press.
DOI: https://doi.org/10.2138/am-2020-7407. http://www.minsocam.org/

Table 1. Details of data collection and structure refinement for K-cymrite and kokchetavite.

Crystal data		
Chemical formula	$KAlSi_3O_8 \cdot H_2O$	$KAlSi_3O_8$
M_r	296.37	278.35
Crystal system, space group	Hexagonal, *P6/mmm*	Hexagonal, *P6/mcc*
Temperature (K)	293	293
a, *c* (Å)	5.3361(3), 7.7081(7)	10.5757(3), 15.6404(6)
V (Å^3)	190.08(3)	1514.94(10)
Z	1	8
Radiation type	Mo *K*α, λ = 0.71073 Å	Synchrotron, λ = 0.2897 Å
μ (mm^{-1})	1.32	1.30
Crystal size (mm)	0.07 × 0.05 × 0.03 mm^3	0.04 × 0.03 × 0.02 mm^3
Data collection		
Diffractometer	Oxford Diffraction Gemini Ultra R	DESY P02.2
Absorption correction	Empirical absorption correction using spherical harmonics	
No. of measured, independent and observed [$I > 2\sigma(I)$] reflections	2415, 127, 124	9272, 1455, 648
R_{int}	0.047	0.035
$(\sin\theta/\lambda)_{max}$ (Å^{-1})	0.662	0.893
Refinement		
$R[F^2 > 2\sigma(F^2)]$, $wR(F^2)$, S	0.040, 0.091, 1.36	0.068, 0.264, 1.14
No. of reflections	127	1455
No. of parameters	17	44
H-atom treatment	H-atom parameters not defined	–
$\Delta\rho_{max}$, $\Delta\rho_{min}$ (e Å^{-3})	0.65, -0.28	0.77, -1.81

Table 2. Structural parameters of K-cymrite and kokchetavite

K-cymrite						
	x	*y*	*z*	U_{eq}	Occupancy	Wyckoff
K1	0	0	1/2	0.0357(9)	1	1b
Si1	2/3	1/3	0.2116(2)	0.0143(5)	3/4	4h
Al1	2/3	1/3	0.2116(2)	0.0143(5)	1/4	4h
O1	1/2	1/2	0.2865(4)	0.0242(9)	1	6i
O2	2/3	1/3	0	0.0202(14)	1	2c
Ow	0	0	0.0386 (17)	0.031(4)	1/2	2e

This is the peer-reviewed, final accepted version for American Mineralogist, published by the Mineralogical Society of America.
The published version is subject to change. Cite as Authors (Year) Title. American Mineralogist, in press.
DOI: https://doi.org/10.2138/am-2020-7407. http://www.minsocam.org/

kokchetavite						
K1	0	0	1/4	0.0346(4)	1	2a
K2	1/2	1/2	1/4	0.0343(3)	1	6f
Si1	0.82106(6)	0.66639(5)	0.39630(3)	0.0174(2)	3/4	24m
Al1	0.82106(6)	0.66639(5)	0.39630(3)	0.0174(2)	1/4	24m
Si2	2/3	1/3	0.39632(6)	0.0233(3)	3/4	8h
Al2	2/3	1/3	0.39632(6)	0.0233(3)	1/4	8h
O1	0.74378(19)	0.75543(17)	0.35856(12)	0.0485(6)	1	24m
O1’	0.7291(2)	0.49937(13)	0.35856(10)	0.0343(4)	1	24m
O2	0.8219(2)	0.6666(2)	1/2	0.0214(4)	1	12l
O2’	2/3	1/3	1/2	0.0264(7)	1	4d

Table 3. Interatomic distances and bond angles for the refined structure of K-cymrite and kokchetavite (the *T* sites are occupied by Al and Si atoms)

Bonds	Bond distances, Å / angles, °
K-cymrite	
K-O1(×12)	3.1349(17)
T-O1(×3)	1.6449(10)
T-O2	1.6312(17)
T-O average	1.6381(16)
O1-T-O1(×3)	108.39(9)
O1-T-O2(×3)	110.53(11)
O-T-O average	109.46(1)
T-O1-T	138.9(2)
T-O2-T	180.0
kokchetavite	
K1-O1(×12)	3.1453(17)
K2-O1(×4)	3.1382(17)
K2-O1’(×4)	2.9617(19)
K2-O1’(×4)	3.327(2)
K2-O1’ average	3.144(18)
T1-O1	1.6363(17)
T1-O1	1.6449(17)
T1-O1 average	1.6406(17)
T1-O1’	1.6421(14)
T1-O2	1.6219(5)
T2-O2’	1.6216(10)
T2-O1'(×3)	1.6458(13)
O1-T1-O1	107.75(12)
O1-T1-O1’	106.92(9)
O1-T1-O1’	108.44(10)
O2-T1-O1’	111.14(10)
O2-T1-O1	111.53(10)
O2-T1-O1	110.90(9)
O-T1-O average	109.45(10)
O2’-T2-O1’(×3)	111.04(6)
O1’-T2-O1’(×3)	107.85(7)
O-T2-O average	109.445(7)
T1-O1-T1	137.51(12)
T1-O2-T1	179.39(14)

This is the peer-reviewed, final accepted version for American Mineralogist, published by the Mineralogical Society of America.
The published version is subject to change. Cite as Authors (Year) Title. American Mineralogist, in press.
DOI: https://doi.org/10.2138/am-2020-7407. http://www.minsocam.org/

T2-O2'-T2	180.0
T1-O1'-T2	136.44(11)

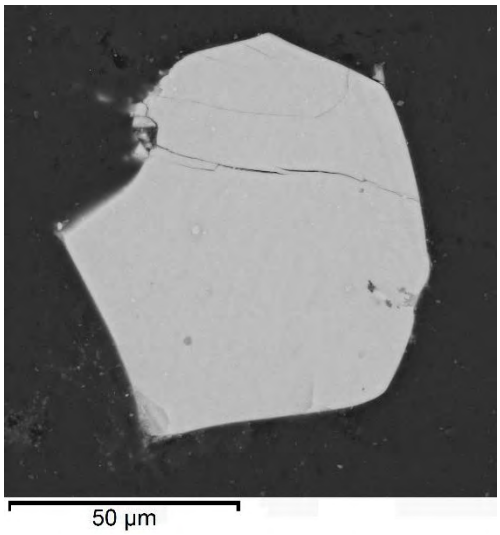

Figure 1. Backscattered electron image of the K-cymrite sample.

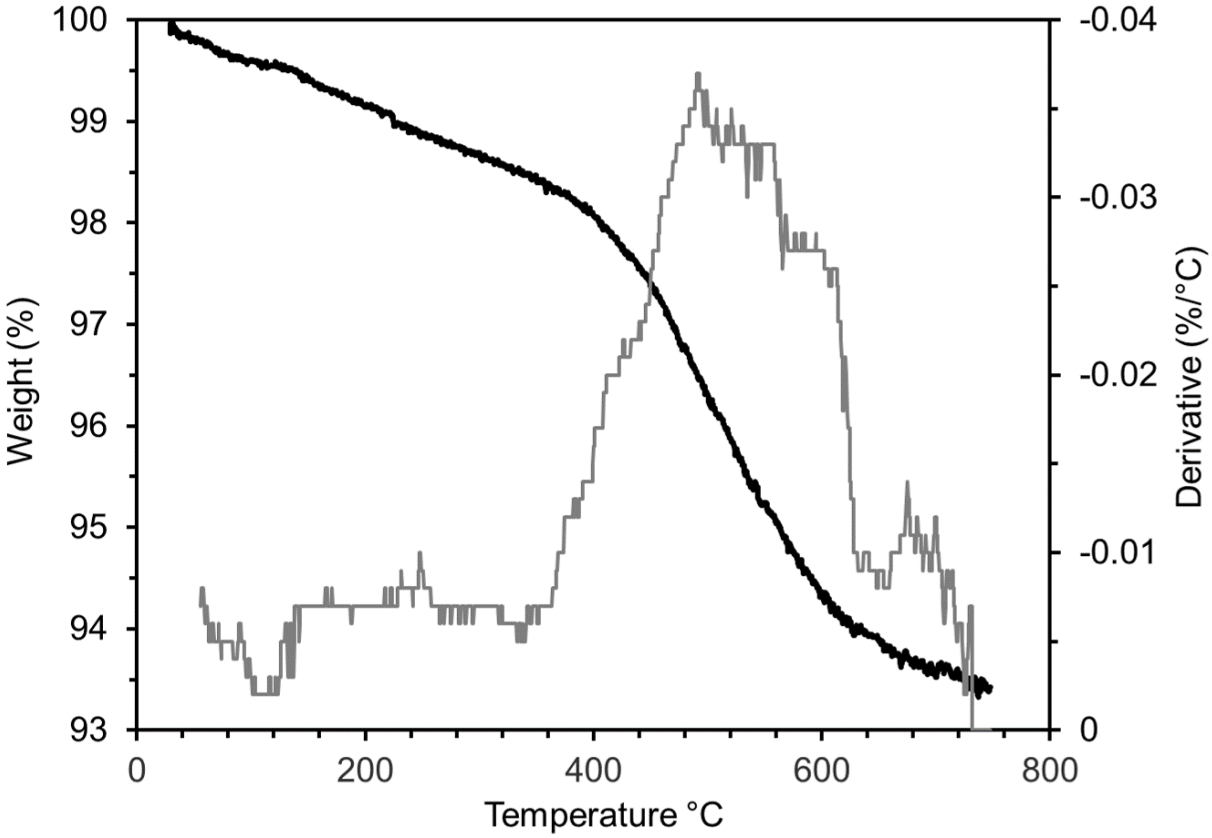

Figure 2. Weight loss (TG) curve and its derivative (DTG) for K-cymrite.

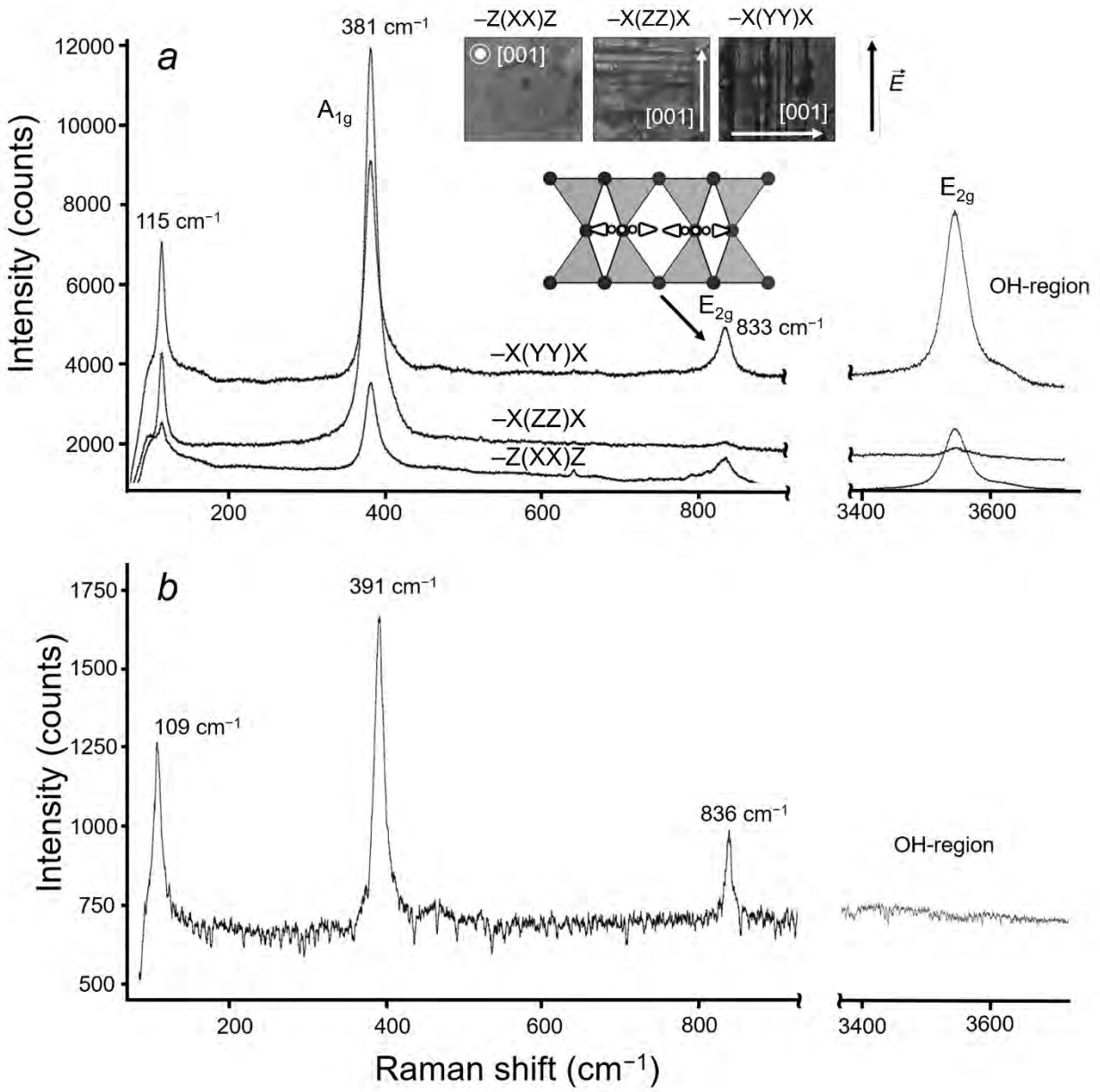

Figure 3. (a) Polarized Raman spectra of K-cymrite; (b) unoriented Raman spectrum of kokchetavite.

This is the peer-reviewed, final accepted version for American Mineralogist, published by the Mineralogical Society of America.
The published version is subject to change. Cite as Authors (Year) Title. American Mineralogist, in press.
DOI: https://doi.org/10.2138/am-2020-7407. http://www.minsocam.org/

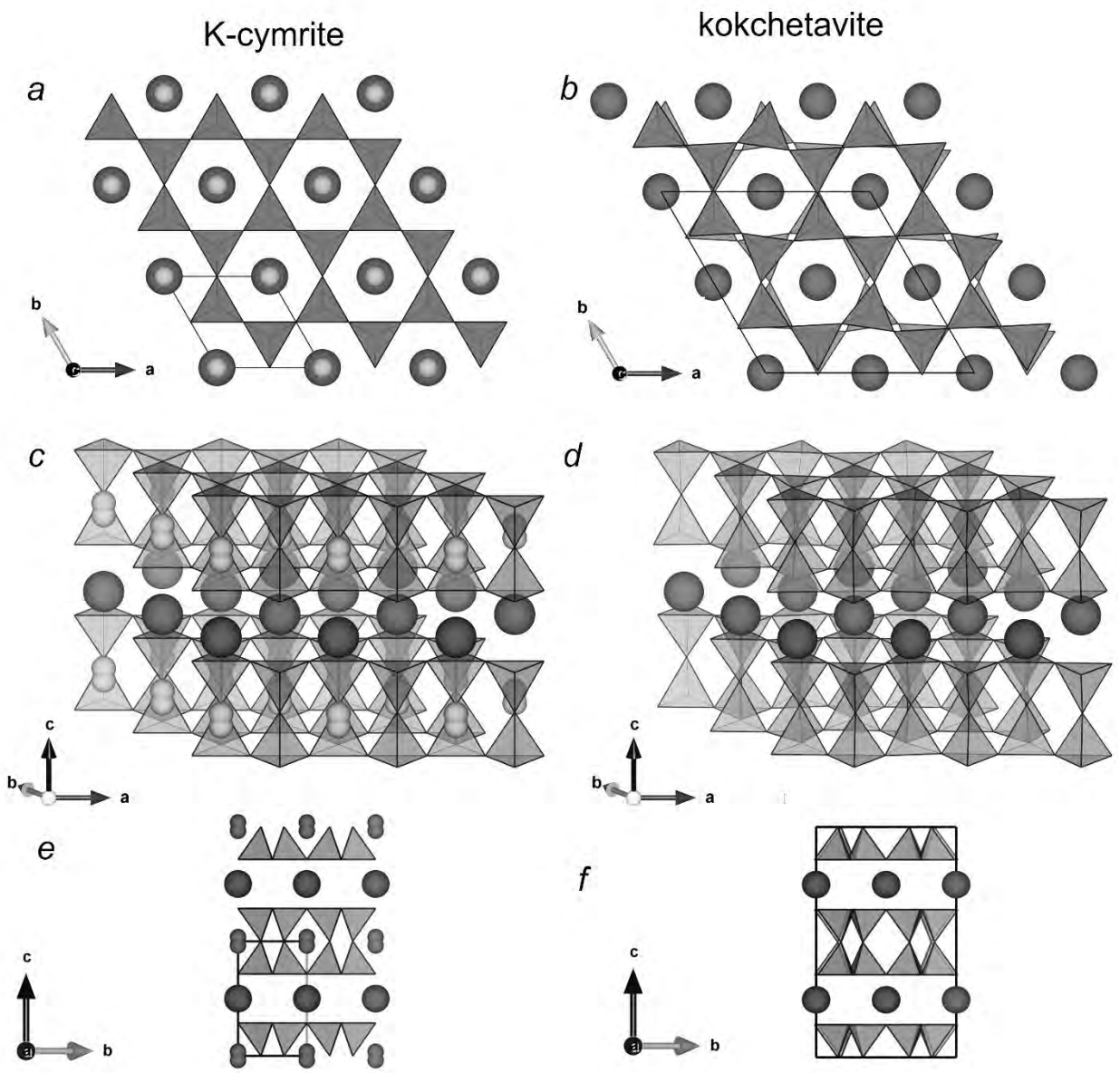

Figure 4. View along [001] direction of K-cymrite (a) and kokchetavite (b) structures; a perspective view of the structures of K-cymrite (c) and kokchetavite (d); view along [100] direction of K-cymrite (e) and kokchetavite (f) structures. The large spheres represent the interlayer K-atoms, the smaller ones – H_2O molecules in the cages inside the double tetrahedral layers.

This is the peer-reviewed, final accepted version for American Mineralogist, published by the Mineralogical Society of America.
The published version is subject to change. Cite as Authors (Year) Title. American Mineralogist, in press.
DOI: https://doi.org/10.2138/am-2020-7407. http://www.minsocam.org/

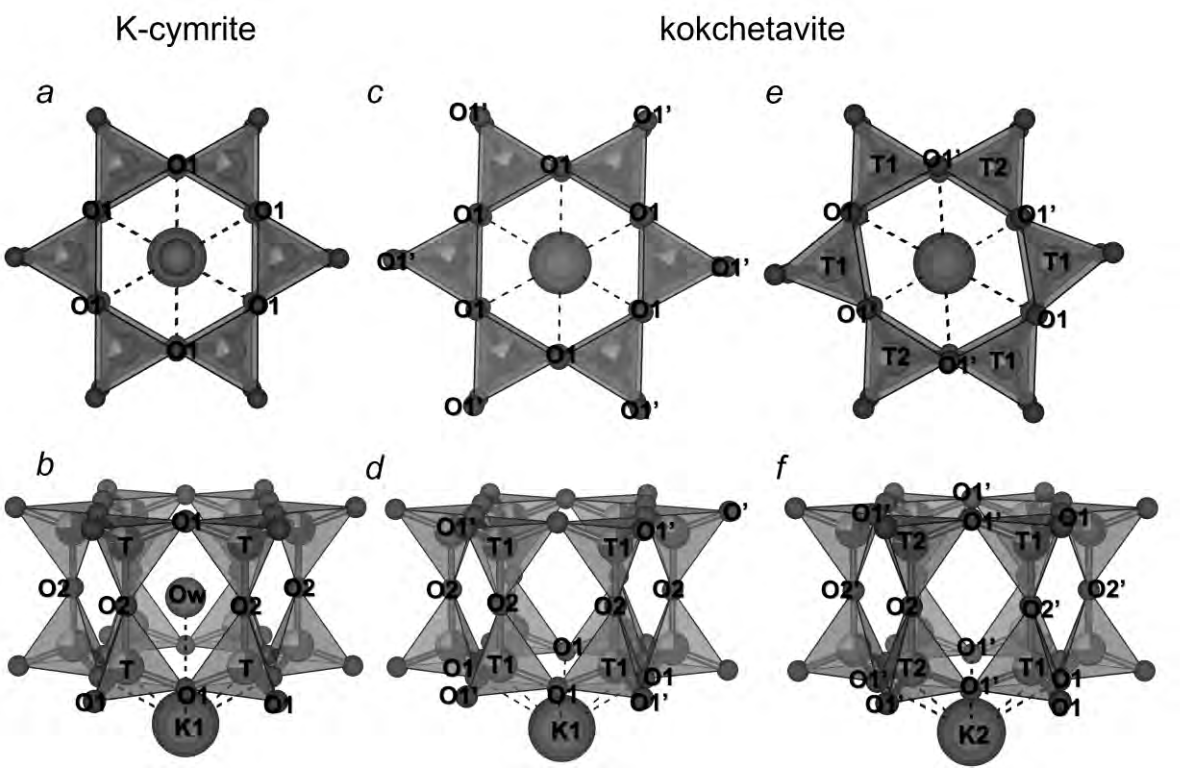

Figure 5. Comparison of K-cymrite (a, b) and kokchetavite (c-f) double rings.

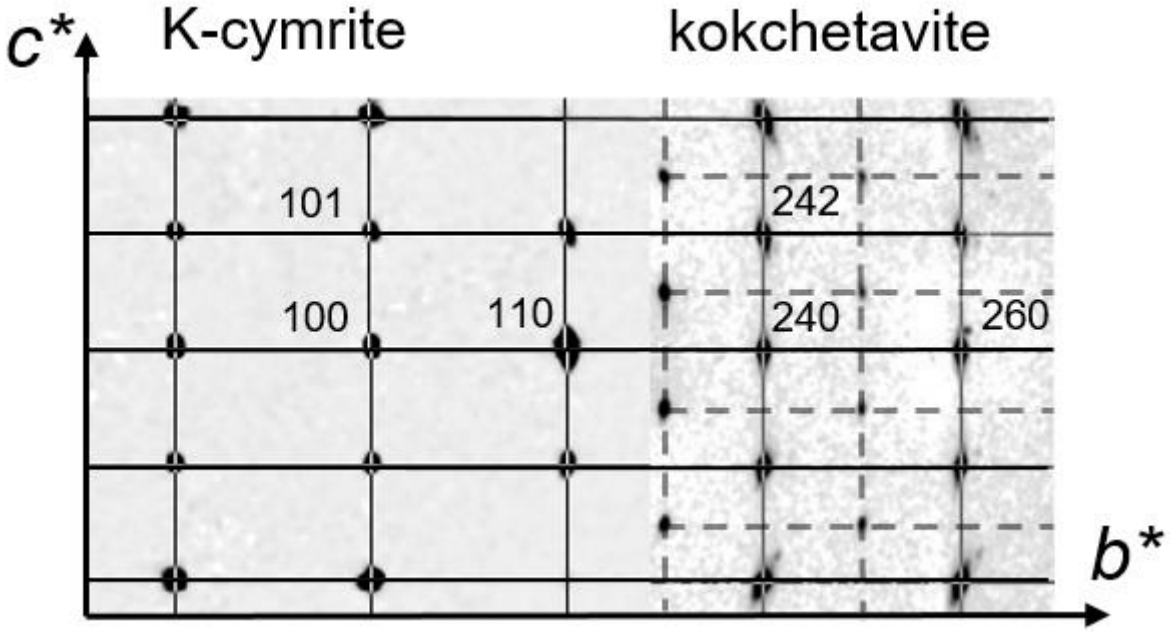

Figure 6. The (1*kl*) plane of the reciprocal lattice of K-cymrite (left) compared with corresponding (2*kl*) plane of kokchetavite (right). Note the absence of $k+l=2n+1$ reflexes in the case of kokchetavite due to a pseudo-A-centering.